Automatic Rectum Limit Detection by Anatomical Markers Correlation

R. Namías[a], J. P. D'Amato[b,c], M. del Fresno[b,d], M. Vénere[b,e]

[a] *CIFASIS, Centre Internacional Franc-Argentin de Sciences de l'Information et de Systmes, UAM (France) / UNR-CONICET, Rosario, Santa Fe, Argentina,*
[b] *Instituto PLADEMA, Universidad Nacional del Centro, Tandil, Argentina*
[c] *Consejo Nacional de Investigaciones Científicas y Técnicas (CONICET), Argentina*
[d] *Comisión de Investigaciones Científicas de la Prov. de Buenos Aires (CIC-PBA), Argentina*
[e] *Comisión Nacional de Energía Atómica (CNEA), Argentina*

Abstract

Several diseases take place at the end of the digestive system. Many of them are diagnosed by means of different medical imaging modalities together with computer aided detection systems. Defining where the rectum ends and the sigmoid colon starts can provide important information to these systems.

An automatic method for rectum and sigmoid colon limit detection is proposed using a novel global curvature analysis on the centerline of the segmented organs. The rectum upper limit is determined through a validation scheme comprising two different anatomical markers: the 3rd Sacral Vertebra and the average rectum length. The method was validated in segmentations performed by a prior hybrid method in both Magnetic Resonance Imaging (MRI) and Computed Tomography Colonography (CTC) acquisitions, obtaining good results. The method is intended for application to the rectum segmentation in MRI for geometrical modeling and as contextual information source in virtual colonoscopies.

Keywords: Anatomical Markers, Colon, Rectum, Computed Tomography, Magnetic Resonance Imaging.

1. Introduction

The lower section of the digestive tube is composed of the colon sigmoid, the rectum and the anus, where several diseases take place. Particularly in the rectum, the most common conditions are partial or complete prolapse and cancer (carcinoma) [1, Ch. 7]. New imaging protocols have recently stood out as common techniques for helping clinicians in the better diagnosis of these illnesses.
On the one hand, CTC is a 3D medical imaging technique that produced a great impact in colorectal cancer (CRC) diagnosis. Actually, the CRC screening tests are grouped into cancer prevention tests and cancer detection tests according to the American College of Gastroenterology [2]. On the other hand, MRI and CT have gained acceptance and reliability in the diagnosis of pelvic organ prolapse thanks to research carried out in the last few years [3, 4, 5].

Computer aided detection (CAD) systems started to play an important role in clinical diagnose. CAD systems were developed in a wide array of medical areas such as cardiology, ophthalmology, dermatology, gynecology, oncology, gastroenterology, etc. In the last decade, many CAD and diagnosis systems have been proposed and actively studied to improve the performance and reliability of human radiologists as second readers [6]. Although there are yet no CAD systems for pelvic organ prolapse, several ones were proposed for colon cancer diagnose in CTC [7, 8, 9].

Extra semantic analysis were made by *Hu et all*[10] to divide lower digestive tube on its base segments (rectum, sigmoid colon, descending colon, transverse colon and ascending colon) in CTC. They used anatomical markers retrieved from the patient's skeleton by performing bone segmentation and user-provided points of reference. This last analysis is fundamental to provide a more detailed description of the context.

In this paper we describe a new procedure for the

Email address: namias@cifasis-conicet.gov.ar (R. Namías)

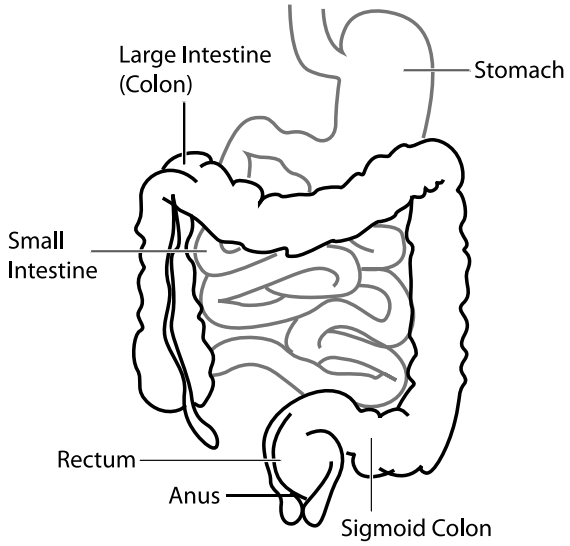

Figure 1: Diagram of the Human Intestine. Drawn by Duncan Lock and released into the Public Domain.

automatic detection of the upper rectum limit. The method is based on a curvature analysis of the segmentation obtained from lower digestive tube and it does not require the user intervention. From 3D images, we obtain a triangular mesh applying an improved *snake* method and then we extract the centerline to get it morphologically analyzed.

Our purposes are not only assisting the colorectal cancer detection as in [10] but also the pelvic prolapse evaluation. We begin reviewing the colon anatomy and the anatomical markers depicted in the literature. Then we outline a brief description of the state-of-art segmentation techniques and centerline extraction employed for CTC acquisitions and the method used in this work. Afterwards, we develop an extensive curvature feature analysis and explore its correlation with the anatomical markers in both CTCs and pelvic volumetric MRIs acquisitions. Finally, we summarize the experimental results and direct future work.

2. Lower Digestive Tube Anatomy

The colon is the last part of the digestive system. It consists of four sections: the ascending colon, the transverse colon, the descending colon, and the sigmoid colon. The cecum, colon, rectum and anal canal make up the large intestine (shown in Fig. 1).

The rectum is about 13 cm long and generally begins in front of the *third sacral vertebra* (S3) (as shown in Fig. 2) as a continuation of the sigmoid colon. It passes downward, following the curve of the sacrum and coccyx, and ends in front of the tip of the coccyx. The lower part of the rectum is dilated to form the rectal ampulla [1].

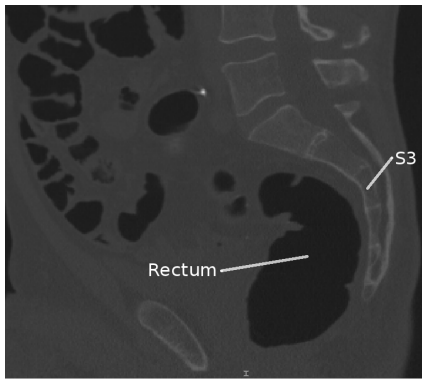

Figure 2: CTC - Sagittal View: 3rd Sacral Vertebra, and Rectum.

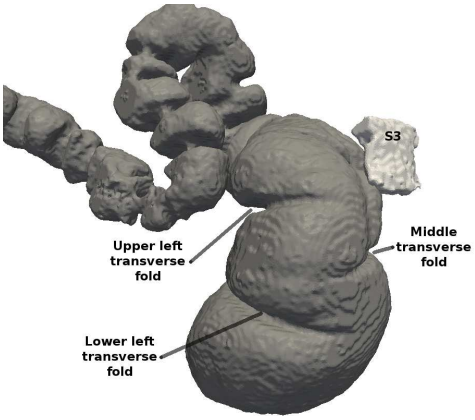

Figure 3: Mesh Representation - Anatomical markers: 3rd Sacral Vertebra (S3), Lower, Middle and Upper transverse folds.

The mucous membrane of the rectum, together with the circular muscle layer, forms two or three semicircular permanent folds called the (lower, middle and upper) transverse folds of the rectum; they may vary in position. In Figure 3 we present the main anatomical markers on a suface mesh segmentation of one CTC acquisition.

3. Materials and Methods

3.1. Medical Data

Unlike other works, we try to generalize a procedure considering studies from two different volumetric imaging modalities: CT and MRI.

The CT colonography collection was downloaded from the National Cancer Institute's Image Cancer

Archive (http://cancerimagingarchive.net/) whereas the MRI acquisitions come from La Timone hospital in Marsille, France.

3.2. Segmentation

For colon segmentation in CTC acquisitions, numerous automatic techniques were proposed in the literature [11, 12, 13]. These techniques are all mainly based on a region growing process with an automatic seed detection and a post processing stage to improve the lumen segmentation which can sometimes may be obstructed by peristalsis, large masses, and/or residual feces. However, these methods are not so useful for the segmentation of the same organs on MRI images.

We propose a more favorable method that could deal with both sorts of studies: a variation of the hybrid active surface method presented in [14] which has been improved with an algorithm for self-collide detection (SCD) described in [15]. The resulting method consists on three main stages. First, a manually seeded region growing (RG) technique is applied to obtain an initial organ segmentation. In the second stage, we convert the RG output to a triangular 3D surface mesh. As the resulting mesh has "staircase" artifacts, it can be smoothed using a Taubin filter, described in [16]. In this third and last stage, we employ a variation of an active surface algorithm with (SCD) which provides the final mesh state.

3.2.1. Robust Active Surface Model

The active surface model, called T-Surface by Mcinerney et al. [17] is used to gather a subvoxel precision segmentation. But when this technique is applied on self-folding organs, several artifacts can show up in the mesh, as inverted o collapsing triangles, that make the mesh useful-less for calculus.

In order to avoid these topological problems we employ the SCD scheme to detect when triangles of the mesh collide or self-intersect.

The evolution starts with a collision-free state. Every a given fixed number of iterations, we check for collisions. This test is made as follows:

1. The triangles are projected over a grid in the $xy-$ *plane*.
2. For every non-empty cell of the grid, all triangles in this cell are tested. If collision occurs, the two triangles are added to a list.
3. Return the list of self-collided triangles.

If the list is empty, it means that the current state is collision-free and the evolution can continue. If not, we do a *rollback* of the whole mesh to the previous checkpoint, freeze the nodes which were involved in the collision and continue evolving. A complete mesh rollback is necessary due to the node neighbor dependance in two of the model forces forces. This procedure ensures that meshes are free from inverted elements in every evolution step.

Anatomical Markers. Organs section discrimination is many times based in spatial observation rules, as "is in front of" or "is behind" a distinguishable part of the body. As we want to delimit the rectum, here we propose to use the S3 anatomical marker as in [10] for the correlation analysis with the gathered analytical features. Therefore, we manually segmented the S3 vertebra using the ITK-SNAP (www.itksnap.org) toolkit.

3.3. Skeletonization

One efficient way to determine the physiognomy of the organ is by extracting what is called the skeleton or centerline. This is a simple way to identify foldings or bends along the studied organ. The skeletonization process is done after the segmentation step. Despite several works directly skeletonize from the voxel mask [18, 19], as our segmentation result is a surface mesh, we employ the *Dijkstra's skeleton algorithm* as proposes *Samara et al.* [20] and employs *Lu et al.* [13] which is more accurate and efficient.

3.4. Curvature Analysis

The skeletonization output is a group of ordered points $\{p_s^i\}$ which describes a polygon in space. We want to analize wheather or not there is a correlation between the bottom digestive tube curves and the S3 anatomical marker which points out the end of the rectum and the beggining of the sigmoid colon.
We propose and study three different approaches for measuring curvature in the tube skeleton: Splines Curvature (SC), Global Splines Curvature (GSC) and Line Mean Differences Curvature (LMDC). Next, we briefly describe each technique and compare their results for the final purpose of detecting the actual curves of the colon.

3.4.1. Splines Curvature

The first curvature analysis approach consists in the differential geometry curvature definition of any parametric curve $\Gamma(t)$. Given a parametric representation of a curve in space, $\Gamma(t) : \mathbf{R} \to \mathbf{R}^3$; the curvature $\kappa(t)$ is defined as:

$$\kappa(t) = \frac{\|\Gamma(t)' \times \Gamma(t)''\|}{\|\Gamma(t)'\|^3} \quad (1)$$

Therefore, for the sake of measuring this magnitude, we generated an extended Catmull-Rom cubic spline passing through the skeleton points $\{p_s^i\}$. As shows [21], is really straightforward to obtain the polynomials and their analytics first and second order derivatives. Hence, we calculate the curvature $\kappa(t)$ over any interpolated point in the spline.

3.4.2. Global Splines Curvature

With the objective of achieving a more macroscopic notion of curvature we propose, instead of computing the κ curvature value for each interpolated point of the spline, to use an odd length sliding window (W_k) over the skeleton points defining a new $\kappa(W_k)$ curvature as:

$$\kappa(W_k) = \left\| \frac{1}{\#(W_k)} \sum_{t \in W_k} \left(\frac{\Gamma(t)' \times \Gamma(t)''}{\|\Gamma(t)'\|} \right) \right\| \quad (2)$$

where k is the window length, $\#(W_k)$ is the amount of interpolated samples in the current sliding window. This new metric have a couple of important differences. First, it is calculated only on each of the p_k points, second it measures the module of the average curvature direction over the spline samples that belongs to W_k and assigns it to the W_k middle point. In this way, we are obtaining a more global information descriptor of the curvature.

3.4.3. Line Mean Difference Curvature

The final approach is radically different from the previous two; it is based on an even more intuitive notion of curvature. We take again an odd length sliding window (W_k) over the skeleton points as in the GPC. Then, a *supporting line* (SL) is sketched among the first and the last point of the window. For all the inner points of the window we obtain the analytic projection over the SL gathering $k-2$ displacement vectors (Figure 4 shows an example). Next, we average these displacement vectors obtaining the mean difference vector (mdv) from the SL and finally we assign the mean difference vector module to the W_k middle point.

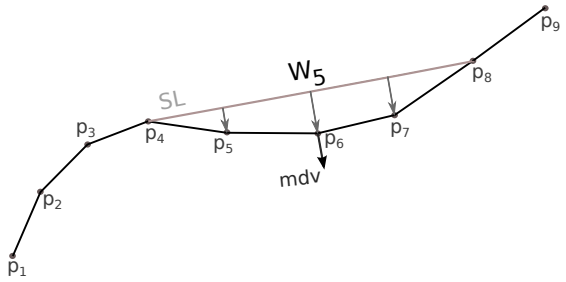

Figure 4: A W_5 sliding window centered in p_6; SL sketched among p_4 and p_8; the 3 displacement vectors between the SL and the inner points $\{p_5, p_6, p_7\}$; and the mean difference vector below p_6.

3.5. Rectum Limit Detection

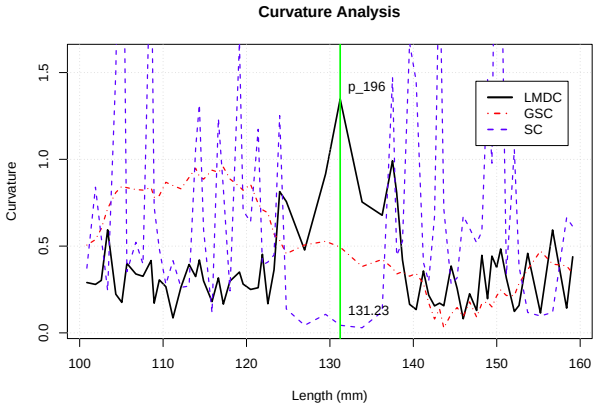

Figure 5: LDCM among the skeleton RI. In green depicted the maximum value (p_s^{196}) 131.23mm away from the end of the rectum.

We are about to find the rectum's limit analyzing the LMDC magnitude among the skeleton. The lower digestive tube could measure more than one meter, having several folds. Therefore, using the skeleton points $\{p_s^i\}$ in the original patients spatial coordinates provided by the DICOM standard we can approximate the path length of the skeleton in milimeters (mm) by adding each skeleton segment length. So, we first restrict the complete interval to the rectum interval (RI) which is the average rectum length $130 \pm 30mm$. Along these line, now we define the limit of the rectum as the point $p_s^i \in RI$ where $LMDC(p_s^i)$ is maximum (see Figure 5).

4. Experimental Results

4.1. Curvature Analysis

The three different curvature measures were explored: SC, GSC and LMDC. The SC measures the instant curvature changes but this metric cannot comprise a macroscopic curvature escenary. Therefore, we tried with the GSC which was supposed to outline the macroscopic curvature of the skeleton. Nevertheless, this idea did not give good results as it could not discriminate accurately the skeleton curves. Finally, using a more intuitive curvature measure as is the LMDC we found the best results. In Figure 6 we show the curvature magnitudes directly over the skeleton inside the segmented tube to visually correlate them with the colon's folds. The color scale goes from red describing high curvature, then white as middle curvature and ending in blue as low curvatures.

Moreover, a curvature curves example among the RI is plotted in Figure 7. On the one side, we can perceive that there is a correlation between the SC (blue) and the LMDC (black) magnitudes in some spots. This analysis points out that the intuitive LMDC measure is not arbitrary and captures the curvature notion. On the other side, whereas the SC has periodic high peaks, the GSC behaves as a low-pass filter having no high peaks all along the RI interval. Therefore, it is difficult in both measures to find an inflexion point which can stand out the curvature position. Finally, we acknowledge that the LMDC measure is the only approach that could accurately find the desired curvatures across the centerline.

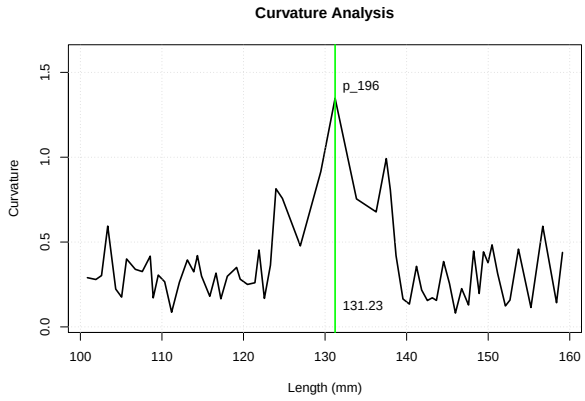

Figure 7: Curvature magnitudes comparison among the RI.

4.2. Anatomical Marker Validation Procedure

The anatomy books outline that the rectum begins in front of the S3 [1]. Therefore we analyze the obtained rectum limit position with its placement near the S3. In order to do that, we place a plane over and below the manually segmented S3 mesh and gather its intersection with the skeleton. We name the intersection interval as the *S3 point interval* (S3-PI). Then, we compare the curvature analysis limits with the anatomical marker validation procedure points to measure the accuracy. In Figure 8 we show

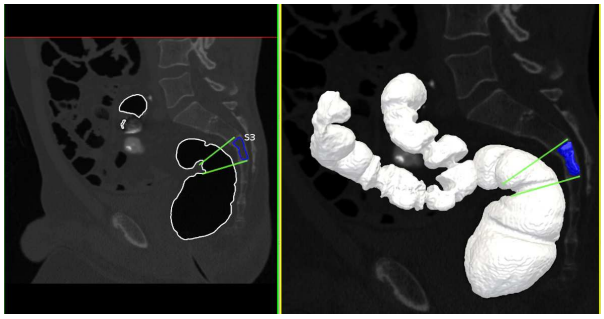

Figure 8: Anatomical Marker Validation Scheme on a CTC.

the proposed validation scheme to evaluate the proposed method. We consider that results are valid when the point limit retrieved by the curvature analysis is within the S3-PI interval. If not, it would be considered that this limit is not in front of the S3 vertebra.

4.3. Real Case Results

We present the technique results applied to two different real imaging diagnosis modalities. The first group consists in a CTC image pack of five patients where there are more than one acquisition for each patient. The second group comprises rectum contrast enhanced ultrafast T2 weighted spin-echo MRIs acquisitions from other four different patients. In general, a complete segmentation of the organ is required for this method to work appropriately. In consequence, some of the available CTC studies from the National Cancer Institute, which were not properly contrasted were not considered.

Table 1 summarizes the experiments. The two groups are divided by an horizontal line. The first two columns represent general aspects: the digestive tube's total length in millimeteres followed by the S3 point interval (S3-PI) that was manually retrieved applying the procedure described in section 4.2. The last column exhibits the rectum limit in mm gathered

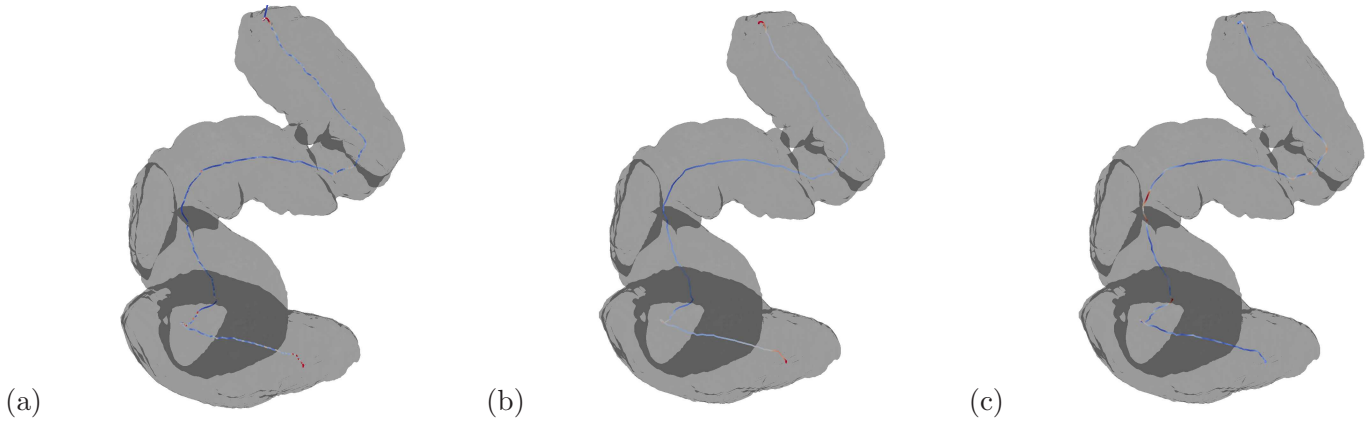

(a) (b) (c)

Figure 6: Curvature Analysis: (a) SC presenting high local variation. (b) GSC depicting low values in high curvature places. (c) LMDC outlining high curvatures accurately.

with the curvature analysis.

Patient	Total Length	S3-PI	Rectum Limit
19_0	676.44	[113.63-140.85]	125.67 ✓
19_1	355.21	[142.80-163.95]	135.76 x
19_2	215.46	[121.53-146.11]	125.99 ✓
20_0	676.44	[113.63-140.85]	125.67 ✓
20_1	1704.72	[84.96-114.81]	108.59 ✓
20_2	575.48	[104.60-127.87]	125.69 ✓
86_0	1808.92	[78.28-111.11]	$106.56^{\dagger}$ ✓
86_1	1775.82	[95.06-122.95]	$101.86^{\dagger}$ ✓
173_1	497.19	[129.15-152.04]	151.05 ✓
173_2	268.48	[112.54-142.54]	131.23 ✓
174_0	1177.34	[90.27-128.85]	106.14 ✓
174_1	678.70	[81.44-127.66]	122.77 ✓
14	154.37	[105.88-128.17]	114.98 ✓
16	155.08	[93.85-118.14]	114.01 ✓
27	137.93	[85.16-112.15]	110.01 ✓
39	305.26	[102.06-127.08]	108.858✓

Table 1: summarizes the experiments. The two image groups are divided by an horizontal line. The second column represent the digestive tube's total length in millimiters. The third one is the (S3-PI) interval that was retrieved applying the procedure described in section 4.2. The last column exhibits the rectum limit in millimeters gathered with the curvature analysis.

The experiments shown in Table 1 depict that the limit points gathered by the proposed curvature analysis are within the S3-PI in almost every study. The rectum length matches the RI as well. For the patient 86 CTC studies† they have their first acquired axial plane over the rectum ending. For this reason, the obtained length is nearby the lower RI limit.
In addition, the 19_1 study was the only case that did not pass the validation. In particular, the centerline returned by the Dijkstra's skeleton algorithm did not fit accurately to the upper left transverse fold causing the analysis to put the limit in the middle transverse fold.

Application example. In Figure 9 we present an example of the method. We show two rectum segmentations one for each imaging modality. In order to find the organ's boundaries in the segmented region, we place a plane perpendicularly to the centerline in the limit point gathered by the proposed method. This plane cuts the surface mesh giving actual ending border of the rectum.

5. Discussion and conclusion

In this paper, we present a novel procedure to automatically obtain the rectum upper limit based only in a curvature analysis of the centerline of the lower digestive tube's segmentation in two different imaging diagnosis modalities. The method was validated using two well known anatomical markers obtaining good results.
The technique was tested on specific segmentation and centerline extraction techniques. However, it can be applied over any which preserves the necessary anatomical characteristics.
We showed a concrete application of this method: rectum delimitation in segmentation tasks. In future works, we plan to extend the analysis to the whole colon to gain realtime organ location information across the virtual colonoscopies in the CTC studies without further processing.

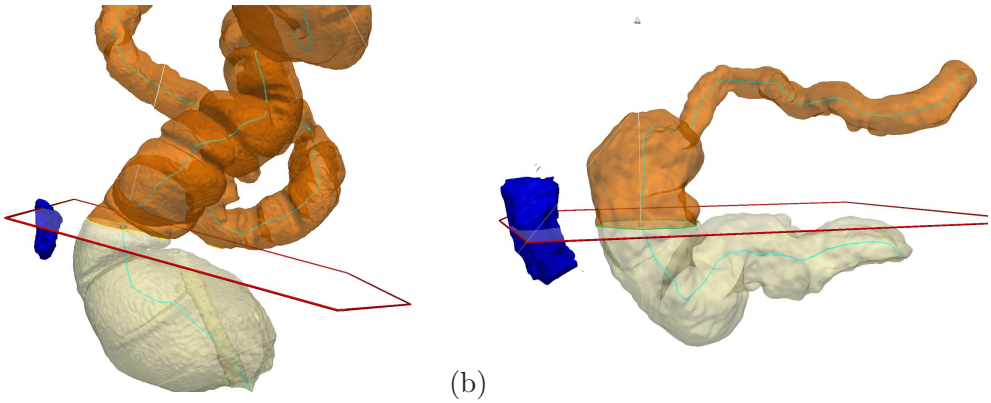

(a) (b)

Figure 9: Rectum segmentation examples using the gathered limits: (a) CTC - Patient 20_1 (limit: 108.59mm). (b) MRI - Patient 39 (limit: 108.86mm).

References

[1] R. S. Snell, Clinical Anatomy by Regions, ninth Edition, Lippincott Williams & Wilkins, 2012, Ch. 7, pp. 766–774.

[2] D. Rex, D. Johnson, J. Anderson, P. Schoenfeld, C. Burke, J. Inadomi, American college of gastroenterology guidelines for colorectal cancer screening 2008, American Journal of Gastroenterology 104 (3) (2009) 739–750.

[3] N. Okamoto, K. Maeda, R. Kato, S. Senga, H. Sato, R. Hosono, Dynamic pelvic three-dimensional computed tomography for investigation of pelvic abnormalities in patients with rectocele and rectal prolapse, Journal of Gastroenterology 41 (8) (2006) 802–806.

[4] H. Pannu, Magnetic resonance imaging of pelvic organ prolapse, Abdominal Imaging 27 (6) (2002) 660–673.

[5] L. Berman, G. Israel, S. McCarthy, J. Weinreb, W. Longo, Utility of magnetic resonance imaging in anorectal disease, World Journal of Gastroenterology 13 (23) (2007) 3153–3158.

[6] M. Giger, H.-P. Chan, J. Boone, Anniversary paper: History and status of cad and quantitative image analysis: The role of medical physics and aapm, Medical Physics 35 (12) (2008) 5799–5820.

[7] T. Chowdhury, P. Whelan, O. Ghita, The use of 3D surface fitting for robust polyp detection and classification in CT colonography, Computerized Medical Imaging and Graphics 30 (8) (2006) 427–436.

[8] H. Yoshida, A. Dachman, Computer-aided diagnosis for CT colonography, in: Seminars in Ultrasound, CT, and MRI, Vol. 25, Elsevier, 2004, pp. 419–431.

[9] L. Lu, M. Wolf, J. Liang, M. Dundar, J. Bi, M. Salganicoff, A two-level approach towards semantic colon segmentation: removing extra-colonic findings, MICCAI (2009) 1009–1016.

[10] Y. Hu, M. S. Ahamed, E. Takahashi, H. Suzuki, Y. Kawata, N. Niki, M. Suzuki, G. Iinuma, N. Moriyama, Segmentation algorithm of colon based on multi-slice ct colonography (2012) 831438–9.

[11] C. Wyatt, Y. Ge, D. Vining, Automatic segmentation of the colon for virtual colonoscopy, Computerized Medical Imaging and Graphics 4 (1) (2000) 1–9.

[12] A. Bert, I. Dmitriev, S. Agliozzo, N. Pietrosemoli, M. Mandelkern, T. Gallo, D. Regge, An automatic method for colon segmentation in CT colonography, Computerized Medical Imaging and Graphics 33 (4) (2009) 325–331.

[13] L. Lu, J. Zhao, An improved method of automatic colon segmentation for virtual colon unfolding, Computer Methods and Programs in Biomedicine 109 (1) (2013) 1–12.

[14] M. del Fresno, M. Vénere, A. Clausse, A combined region growing and deformable model method for extraction of closed surfaces in 3D CT and MRI scans, Computerized Medical Imaging and Graphics 33 (5) (2009) 369–376.

[15] R. Namías, J. D'Amato, M. Del Fresno, M. J. Vénere, Mesh generation of pelvic organ surfaces using active contours with self-collision detection, Mecánica Computacional XXXI (2012) 3062–3074.

[16] G. Taubin, A Signal Processing Approach to Fair Surface Design, Computer Graphics 29 (Annual Conference Series) (1995) 351–358.

[17] T. Mcinerney, D. Terzopoulos, Topology adaptive deformable surfaces for medical image volume segmentation, IEEE Transactions on Medical Imaging 18 (1999) 840–850.

[18] R. J. Sadleir, P. F. Whelan, Fast colon centreline calculation using optimised 3D topological thinning, Computerized Medical Imaging and Graphics 29 (4) (2005) 251 – 258.

[19] C. Arcelli, G. Sanniti Di Baja, L. Serino, Distance-driven skeletonization in voxel images, IEEE Transactions on Pattern Analysis and Machine Intelligence 33 (4) (2011) 709–720.

[20] Y. Samara, M. Fiebich, A. Dachman, J. Kuniyoshi, K. Doi, K. Hoffmann, Automated calculation of the centerline of the human colon on CT images, Academic Radiology 6 (6) (1999) 352–359.

[21] E. Catmull, R. Rom, A class of local interpolating splines, Computer aided geometric design. Academic Press. (1974) 317–326.

Rafael Namias received his B.S. degree in Computer Science from Rosario National University, Rosario, Argentina, in 2007. He is currently a Ph.D. Candidate in Centro Internacional Franco Argentino de Ciencias de la Información y Sistemas (CIFASIS). His research interests are in the areas of medical imaging, segmentation, and features analysis.

Juan Pablo D'Amato is Phd in Computational and Industrial Mathematics since 2011 at the UNICEN University (Tandil, Argentina). Hes professor assistant in Computer Graphics courses and has worked in the development of real time systems and simulators for the Argentine Army Forces. His main research interests include geometry, high performance in GPUs, visualization and virtual reality applied to training.

Mariana del Fresno received her PhD (2008) at the UNICEN University (Tandil, Argentina). Currently she is professor in the Department of Computer Science at the same University and member of the Comisión de Investigaciones Científicas de la Provincia de Buenos Aires. Her research interests include medical image processing, segmentation and visualization.

Marcelo Vénere is a PhD in Nuclear Engineering from Balseiro Institute, Argentina. Hes an Associated Professor in Computer Graphics and Algorithms courses at the UNICEN University (Tandil, Argentina). He is leading several projects in arterial fluid simulation, real time training and computer graphics; among other topics. He is the Co-Director of the PLADEMA Research Institute of the UNICEN University at Tandil, Argentina.